Chemical Engineering Journal 418 (2021) 129421

Contents lists available at ScienceDirect

Chemical Engineering Journal

journal homepage: www.elsevier.com/locate/cej

# Facile one-pot synthesis of rod-coil bio-block copolymers and uncovering their role in forming the efficient stretchable touch-responsive light emitting diodes

Dai-Hua Jiang [a,b,c,1], Brian J. Ree [d,1], Takuya Isono [d], Xiao-Chao Xia [d,e], Li-Che Hsu [b,c], Saburo Kobayashi [b], Kuan Hoon Ngoi [f,g], Wei-Cheng Chen [a], Chih-Chun Jao [a], Loganathan Veeramuthu [a], Toshifumi Satoh [d,*], Shih Huang Tung [c,*], Chi-Ching Kuo [a,*]

[a] Institute of Organic and Polymeric Materials, Research and Development Center of Smart Textile Technology, National Taipei University of Technology, Taipei 10608, Taiwan
[b] Graduate School of Chemical Sciences and Engineering, Hokkaido University, Sapporo 060-8628, Japan
[c] Institute of Polymer Science and Engineering, National Taiwan University, 106 Taipei, Taiwan
[d] Faculty of Engineering, Hokkaido University, Sapporo 060-8628, Japan
[e] School of Materials Science and Engineering, Chongqing University of Technology, Chongqing 400054, China
[f] Materials Science Program, Department of Applied Physics, Faculty of Science and Technology, Universiti Kebangsaan Malaysia, Bangi 43600, Selangor, Malaysia
[g] Department of Chemistry and Pohang Accelerator Laboratory, Pohang University of Science and Technology, Pohang 37673, North Korea

ARTICLE INFO

*Keywords:*
Polyfluorene
Rod-coil conjugated block copolymer
Smart synthesis
Light-emitting diode
Flexible wearable device

ABSTRACT

Bio-derived optoelectronic material is captivating and sustainable research as it reduces the environmental toxicity and comforting the wearable aspects. Our research involves the synthesis of series of bio-derived polyfluorene-*block*-poly(*δ*-decanolactone) (PF-*b*-PDL) conjugated block copolymers through smart one-pot procedure that involves simple purification for fabricating touch-responsive light-emitting diode (LED) devices. Compared with PF homopolymer, the block copolymers exhibit higher photoluminescence quantum yields and higher exciton binding energies. $PF_{18}$-*b*-$PDL_{13}$ specifically exhibits external quantum efficiency (EQE %) (~6 times higher than PF homopolymer). Moreover, because of coily PDL block inducing a highly stable bound state in block copolymer generating the increment in PL lifetime and exciton binding energies than the homopolymer. Furthermore, the diblock copolymers device exhibits fully solution processability, higher carrier recombination efficiency, flex-stretch stability, good structural integrity and mechanical endurance highlighting the brighter potential of our bio-derived block copolymers for fabricating highly durable wearable stretchable nano and microelectronic devices.

## 1. Introduction

Conjugated block copolymers (BCPs) have attracted a considerable amount of interest from academia and industry for their wide ranging applications in nano-microelectronics,[1] optoelectronics,[2–8] biotechnology,[9,10] and environmental technology.[11] Given their nature to self-assemble into phase separated nanostructures, various types of morphologies such as spherical,[12,13] cylindrical,[13,14] bicontinuous,[13,15] and lamellar nanostructures[13,16] of conjugated BCPs have been reported thus far. The type and size of self-assembled nanostructures are controlled by overall molecular weight and volume fraction between the blocks. By taking this bottom-up approach in modifying the active-layer phase consisting of the conjugated block, the overall performance level of block copolymer devices can be fine-tuned for specific purposes. In particular, polyfluorene (PF) is a deep blue light-emitting conjugated polymer with a good photoluminescence quantum yield and an excellent thermal stability, and solution processability.[17–21] PF-based conjugated BCPs containing dielectric, coily blocks are reported to have enhanced PF crystallinity,[22,23] structural ordering,[14,22,24] and stretchability.[24,25] The control over domain size of nanostructures to achieve an exciton diffusion length of 20–50 nm is known to optimize device performance levels.

* Corresponding authors.
*E-mail addresses:* satoh@eng.hokudai.ac.jp (T. Satoh), shtung@ntu.edu.tw (S. Huang Tung), kuocc@mail.ntut.edu.tw (C.-C. Kuo).
[1] Contributed equally to this work.

https://doi.org/10.1016/j.cej.2021.129421
Received 17 January 2021; Received in revised form 7 March 2021; Accepted 15 March 2021
Available online 21 March 2021

[26,27] In addition, coil blocks add stretchability to the overall BCPs and enable the construction of wearable devices.[28,29] However, the insulating property of coil blocks considerably dampens the interchain charge transport properties, which is unfavorable for achieving efficient electroluminescent device. Therefore, a tradeoff exists in the molecular design of conjugated BCPs and it is of urgent need to solve this tradeoff to develop wearable stretchable optoelectronics devices.

Typically, PF derivatives are synthesized through Suzuki–Miyaura polycondensation in a classical step-growth manner but it is unsuitable for producing BCPs. As an alternative, Suzuki–Miyaura catalyst transfer polymerization (SCTP) enables BCP synthesis through the controlled chain-growth of PF that is end-functionalized with chemically reactive groups for copolymerization.[2,3,30] In general, ethynyl or azido end groups are used to produce PF-based BCPs through click chemistry.[10,25] However, the complex synthesis and stringent purification procedures involved in the aforementioned methods inhibit the mass production of BCPs.[2,10,22,25,30,31] Despite the limitations, some studies have utilized those methods to demonstrate successful application of conjugated BCPs. Chen *et al.* reported the synthesis of poly[2,7-(9,9-di-*n*-hexylfluorene)]-*b*-poly(*n*-butyl acrylate) (PF-*b*-PBA) rod-coil diblock copolymers through a click reaction. These copolymers exhibit excellent fluorescence properties as well as high deformability, which demonstrate reliable high-performance wearable electronic devices.[22] Moreover, Chiu *et al.* designed intrinsically elastic PF-based copolymers through reversible addition–fragmentation chain transfer polymerization and it exhibited highly durable photoluminescence quantum yield (PLQY) even at 300% strain over 100 cycles.[24] Aforementioned studies have shown that conjugated BCPs exhibit higher PLQY than their respective homopolymers.[22,24] Therefore, conjugated BCPs are potential candidates for light-emitting diode (LED) applications. However, in-depth investigation regarding higher PLQY in BCPs molecular systems has not been reported yet.

To address the limitations in synthetic strategy complication, purification and sustainable bio-derived molecular blocks to construct conjugated BCPs with better PLQY, this study reports a smart scalable one-pot synthesis of poly(9,9-di-*n*-hexyl-2,7-fluorene)-*block*-poly(*δ*-decanolactone) (PF-*b*-PDL), poly(9,9-di-n-hexyl-2,7-fluorene)-*block*-[(phthalic anhydride)-*alternative*-(ethyl glycidyl ether)] (PF-*b*-(PA-*alt*-EGE)), and poly(9,9-di-n-hexyl-2,7-fluorene)-*block*-[(allyl succinic anhydride)-*alternative*-(ethyl glycidyl ether)] (PF-*b*-(AA-*alt*-EGE)) by using SCTP and ring-opening polymerization (ROP). High PLQY and exciton binding energy (EBE) were induced by a weak screening effect from PDL blocks in which their low dielectric constant increases the attractive force between electrons and holes interacting in PF blocks. The LED devices with PF-*b*-PDL as the emissive layer exhibit good mechanical robustness (stable 300 touch responses) and a greater external quantum efficiency (EQE % or 6 times higher) than devices with PF homopolymer. The results demonstrate conjugated BCP LED devices exhibiting superior performance over their conjugated homopolymer counterparts.

## 2. Experimental section

### 2.1. Materials:

Potassium 2-(7-bromo-9,9-di-*n*-hexyl-9H-fluorene-2-yl) triolborate was prepared according to a previous report.[32] Tris-(dibenzylideneacetone) palladium ($Pd_2(dba)_3$, >97%), tetrahydrofuran (THF, anhydrous, ≥99%), methanol (MeOH, ≥99%), dichloromethane ($CH_2Cl_2$, anhydrous, ≥99%), toluene (anhydrous, ≥99%), chloroform ($CHCl_3$, anhydrous, ≥99%), *δ*-decanolactone (*δ*-DL), phthalic anhydride (PA), ethyl glycidyl ether (EGE), *tert*-butylimino-tri(pyrrolidino)phosphorene (*t*-Bu$P_1$) and allyl succinic anhydride (AA), dec-5-ene (TBD, >98.0%), poly(9,9-di-*n*-octyl-2,7-fluorene) (PFO) ($M_n \sim 10{,}000$, $Đ \sim 2$), and poly(ethylene glycol) (PEO) were purchased from Sigma-Aldrich. Tri(*tert*-butyl)phosphine (*t*-$Bu_3P$, >96%) was obtained from Wako Pure Chemical Industries, Ltd. 4-Iodobenzyl alcohol (>99.0%) was bought from Tokyo Chemical Industry Co., Ltd. Poly(3,4-ethylenedioxythiophene)-poly(styrenesulfonate) (PEDOT: PSS; high conductivity grade 1.1 wt% in $H_2O$) was purchased from Ossila, Ltd. Polyurethane (PU) was purchased from RainEmpire Taipei Co., Ltd. Silver nanowires (average diameter = 55–75 nm, average length = 20–40 μm) dispersed in IPA (0.66%) were purchased from Zhejiang Kechuang Advanced Materials Co., Ltd.

### 2.2. Synthesis of PF-based block with ROP monomer via smart procedure

The typical polymerization procedure is as follows: An appropriate amount of TBD (0.026 mmol, 1 equiv.), 4-iodobenzyl alcohol (0.026 mmol, 1 equiv.), and *δ*-DL (1.538 mmol, 60 equiv.) were added to an oven-dried Schlenk flask equipped with a magnetic stir (The PA or AA is 0.513 mmol, 20 equiv with EGE (1.026 mmol, 40 equiv) is added) The Schlenk flask was placed in an aluminium heating block with predetermined temperature of 25 °C to start the ROP (100℃ for the PA or AA with EGE). During the ROP step, a crude aliquot was withdrawn from the system by pipette and monitor by $^1$H NMR spectroscopy and size exclusion chromatography (SEC) to determine monomer conversion and molecular weight. After the defined time, $Pd_2(dba)_3{\cdot}CHCl_3$ (0.010 mmol, 0.4 equiv.), *t*-$Bu_3P$ (0.057 mmol, 2.2 equiv. as 0.5 mol $L^{-1}$ stock solution in tetrahydrofuran (THF)), and dry-THF (12 mL) were added to the reaction mixture, and stirred for 30 min to form Pd-initiator complex. A solution of HexFL (0.466 mmol, 18 equiv.) in dry-THF (200 mL) was introduced to the Pd-initiator solution, which had been purged with argon and pre-cooled at − 10 °C, by a cannula to start the SCTP for 10 min. To terminate the polymerization, 12 M hydrochloric acid (HCl) (10 mL) was added to the reaction mixture and react for 30 min. SEC was performed to trace the final copolymers. The elution peaks of the copolymers shifted to a shorter elution time than those for the corresponding I-PDL$_n$, which indicated a successful chain extension of the PF block. After removing the solvent by evaporation, the residue was dissolved in $CH_2Cl_2$ and washed with brine. The organic layer was dried over $MgSO_4$ and purified by alumina column. The residue was diluted by adding THF and poured into cold acetone. The precipitate was collected by filtration and dried under reduced pressure to get $PF_{18}$-*b*-$PDL_{36}$ (yield: 63.1%) as a dark green powder. $M_{n,NMR}$ = 12,800 g $mol^{-1}$; $Đ$ = 1.311. $^1$H NMR (400 MHz, $CDCl_3$): *δ* (ppm) 7.71–7.83 (m, Ar-H of PF backbone), 5.18 (d, $-CH_2OH$): 2.29 (br, $-CH_2(CH_2)_4CH_3$ of PF side chain), 0.79–1.27 (m, $-CH_2(CH_2)_4CH_3$ of PF side chain), 4.87 (br, PDL backbone and side chain connection), 1.27–2.29 (br, PDL backbone), and 0.87–1.55 (br, pentyl side chain of PDL).

### 2.3. Touch-responsive light-emitting diode device fabrication

The PU substrates were prepared by being spin-coated onto the polytetrafluoroethylene (PTFE) substrate and being cured at 40 °C for 1 day. The PU substrates were oxygen plasma treated for 3 min and the PEDOT: PSS/ poly(ethylene glycol) (PEO) (5 wt%) solution was spin-coated onto the treated PU substrate at 1000 rpm for 30 s. Subsequently, the film was annealed at 80 °C for 15 min to remove residual solvents. After being cooled down, the substrate was transferred into a nitrogen-filled glove box and spin-coated with the PF-based block copolymer, as an emissive layer. The emissive layer was prepared by spin coating at 3000 rpm for 60 s and annealed at 120 °C in vacuum for 1 day, and then, the spacer PET was introduced onto the emissive layer. The prepared PU@AgNWs electrode was then faced down and stacked onto the emissive layer that plays the role of cathode (upper electrode).

### 2.4. Characterization

$^1$H, $^{13}$C, COSY, HMQC, and DOSY NMR spectra were measured with a JEOL JNM-ECS 400 (JEOL Ltd., Tokyo, Japan) at room temperature at 400 MHz in chloroform-$d_1$, and chemical shifts are referenced to an internal standard. SEC analyses are using THF as the eluent at a flow rate

of 1.0 mL $min^{-1}$ at 40 °C and measured by employing a JASCO (JASCO Co., Tokyo, Japan) high performance liquid chromatography system (PU-980 Intelligent HPLC pump, CO-2065 Plus Intelligent Column Oven, RI-2031 Plus Intelligent RI Detector, and DG-2080–53 Degasser) equipped with a Shodex KF-G guard column (4.6 mm × 10 mm; particle size, 8 μm) and two Shodex KF-804L columns (linear; particle size, 7 μm; 8.0 mm × 300 mm; exclusion limit, 4 × 104) (Showa Denko K. K., Tokyo, Japan). The calculated number average molecular weight ($M_{n,SEC}$) and dispersity ($Đ$) of the polymers were calibrated with polystyrene (PSt) standards. UV–visible spectra were measured by Jasco V-370 spectrophotometer (JASCO Co., Tokyo, Japan). The PL spectra were measured by a Fluorolog-3 spectrofluorometer (Horiba Jobin Yvon, Paris, France), and the polymer films were excited at wavelengths of 365 nm. The structure of the polymer thin films was imaged by Hitachi AFM5000II (Hitachi Systems Co., Ltd., Tokyo, Japan) operating in tapping mode under an ambient atmosphere. The thin films for the AFM measurements were prepared by spin coating (3000 rpm, 60 s) from the polymer solutions in THF (5.0% w/w) onto a silicon substrate. The thin film samples were annealed under vacuum at 120 °C for one day. The AFM images were processed using Gwyddion software. DSC was measured to investigate thermal properties under a nitrogen atmosphere by Hitachi DSC 7000X (Hitachi High-Tech Science Co., Ltd., Tokyo, Japan) with a heating/cooling rate of 10 °C $min^{-1}$ from − 100 °C to 250 °C under a nitrogen flow. TGA was performed through a Bruker AXS TG-DTA2010SAT (Bruker AXS, Billerica, USA) with a heating rate of 10 °C $min^{-1}$ from 100 °C to 500 °C under a nitrogen flow. Synchrotron GIWAXS measurements were conducted with an X-ray beam of wavelength ($\lambda$) 0.12359 nm at the 3C beamline[33–36] of the Pohang Accelerator Laboratory (PAL), Pohang, Korea. A 2D charge-coupled detector (model Eiger X 4 M, DECTRIS Ltd., Baden-Daettwil, Switzerland) was used to measure all GIWAXS data. The incidence angle $\alpha_i$ of the X-ray beam with respect to the film sample surface was set in the range 0.093–0.196°, which is between the critical angle of the polymer film and the silicon substrate ($\alpha_{c,f}$ and $\alpha_{c,s}$). Aluminium foils were used as a semi-transparent beam stop. The sample-to-detector distance (SDD) was set to 208.3 mm. Each scattering pattern was collected for 30 s. The scattering angles were corrected according to the positions of the X-ray beams reflected from the silicon substrate as well as using precalibrated silver behenate standards (Tokyo Chemical Inc., Tokyo, Japan). Absolute PLQY measurement was recorded by using Enli Tech LQ-100X (Enli Technology Co., Ltd., Kaohsiung, Taiwan) for detecting all-polymer thin films under different strains or stretching cycles through the integrating sphere at a fixed excitation wavelength at 365 nm. A measurement is done of the fluorescence emission ($E_c$) and the scatter ($L_c$) of the samples and also the emission and scatter of a blank ($L_a$ and $E_a$). Finally, the absolute PLQY can be calculated from the equation of $\Phi_f = \frac{E_c - E_a}{L_a - L_c}$. The highest occupied molecular orbital (HOMO) energy levels were calculated from ultraviolet photoelectron spectroscopy (UPS), whereas the lowest unoccupied molecular orbital (LUMO) energy levels were estimated from the difference between the optical band gap and HOMO level based on the equation LUMO (eV) = HOMO + $E_g^{opt}$. The OM observation was measured under a microscope by LSM 21 510 Meta (ZEISS Co., Ltd., Oberkochen, Germany) equipped with a 22 LCI Plan-Neofluar 40x $1.3^{-1}$NA immersion. The Commission Internationale de l'éclairage (CIE) color coordinates and correlated color temperature (CCT) of the LED spectra were measured by PR670 spectroradiometer (Titan Electro-Optics Co., Ltd., Taipei, Taiwan) under ambient air conditions at 25 °C. The calibration method was standard sunset light, which correlated to a color temperature of 2856 K, to confirm instrument correctness. The TR-PL spectra were coupled to a Horiba iHR320 spectrometer (HORIBA, Kyoto, Japan) with a Hamamatsu C10910 streak camera and an M10913 slow single sweep unit. Temperature-dependent photoluminescence was measured with a pulsed diode-laser by PicoQuant LDH-D-C-375 (PicoQuant, Berlin, Germany) at a repetition rate of 1 MHz.

### 2.5. Arrhenius formula simulation of the binding energy

Here, the photo-generated excitons are assumed to be depopulated only by thermal dissociation and radiative recombination. In the steady-state PL measurement, the $n_{Pg}$ refers to the number of photo-generated excitons, $n_{PL}$ is the number of the radiative emissions induced by the exciton recombination, which can be determined from the integrated PL intensity, and $n_{td}$ is the number of thermally dissociated excitons. According to the Arrhenius formula, $n_{td}$ is saturated when the $T$ is not too high and the $n_{td}$ $\hat{I} \pm$ $Ae^{-E_b/kT}$ can get, in which $E_b$ is the binding energy and $k$ is the Boltzman constant. Assuming that when $T = \infty$ it has $n_{PL} = 0$, then $n_{PL} = n_{Pg} - n_{td} = A(1 - e^{-E_b/kT})$. After fitting $n_{td}(T)$, we can determine $A$ and $E_b$.

$$n_{PL} = n_{pg} - n_{td} = A(1 - e^{-E_b/kT}) \quad (1)$$

### 2.6. The time decay curve fitting by exponential function

The decays are fitted with the formula (2) where $\tau_1$ is the time constant, which is attributed to the intrinsic recombination and $A_1$ is the fractions of the contribution. The first 1.0 ns following the laser excitation are used for fitting. The time constant of all the dots that have measured is around 0.0 ~ 1.0 ns. If the time constant is determined by a nonradiative channel, the distribution of exciton would expect a more rapid decline in time constant.

$$F(t) = A_1 e^{-t/\tau_1} \quad (2)$$

## 3. Results and discussion

### 3.1. Synthesis and characterization of PF-based block copolymer

The details of the one-pot synthesis of PF-based BCPs are given in the Supporting Information, and the molecular characteristics are summarized in Table S1 (Supporting Information). The smart one-pot synthesis is a two-step process based on the ROP of bio-based sugar derived $\delta$-decanolactone ($\delta$-DL) and SCTP of potassium 2-(7-bromo-9,9-di-*n*-hexyl-9H-fluorene-2-yl) triolborate (HexFL) carried out in a sequential manner (Fig. 1a). To realize the one-pot process, commercially available 4-iodobenzyl alcohol possessing hydroxyl and iodobenzene groups was chosen as the appropriate difunctional initiator. The hydroxyl group functions as the initiating site for ROP, and the iodobenzene group reacts with Pd(0) to form an initiating site for SCTP. First, ROP of $\delta$-DL performed in bulk was carried out by using 1,5,7-triazabicyclo[4.4.0]dec-5-ene (TBD) as a catalyst and 4-iodobenzyl alcohol as an initiator at 25 °C under a nitrogen atmosphere to produce iodo-end-functionalized PDLs [I-PDL$_n$ ($n$ = 13, 24, and 36; Fig. 1a,b)]. The molecular weight of I-PDL$_n$ was controlled by varying the reaction time and $\delta$-DL/initiator ([$\delta$-DL]$_0$/[I]$_0$) ratio. The ROP monitored by performing SEC and $^1$H nuclear magnetic resonance (NMR) analysis of aliquots at regular intervals produced a linear correlation between the evolution of the molecular weight ($M_{n,SEC}$) and monomer conversion, which demonstrated a living polymerization behaviour (Figs. S1–S3 and Table S2, Supporting Information). Subsequent addition of a mixture of a tris(dibenzylideneactone) dipalladium (0)-chloroform adduct ($Pd_2(dba)_3{\cdot}CHCl_3$) and tri-*tert*-butylphosphine (*t*-$Bu_3P$) resulted in the formation of a coordination complex with I-PDL$_n$ for initiating a controlled chain-growth SCTP of HexFL. To understand the effect of the molecular weight balance between the conjugated rod and coil blocks on the LED performance, the PF blocks in all copolymers were synthesized with a fixed number average molecular weight ($M_{n,NMR}$) of 6,300 g $mol^{-1}$ (i.e., 18 repeating units).[37] On the other hand, the ring-opening alternating copolymerization (ROAC) of epoxides with cyclic anhydrides has been recognized as a promising approach to diversified polymers and allowing facile functional tunability. In view of achieving facile approach, the utilized commercially available initiator bridges two different catalytic

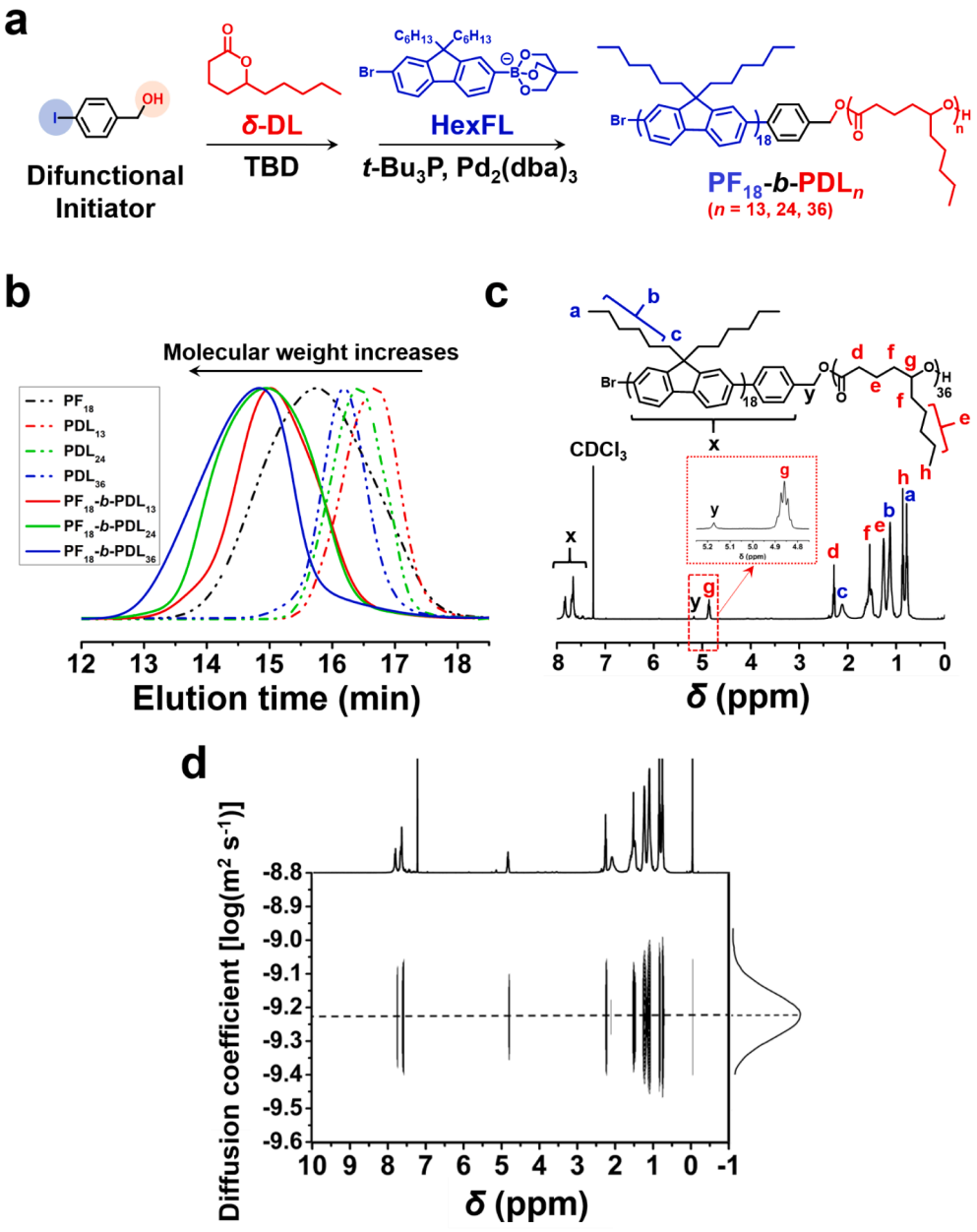


**Fig. 1.** Formation and structure confirmation of $PF_{18}$-*b*-$PDL_n$ block copolymers. (a) Smart synthesis of $PF_{18}$-*b*-$PDL_n$ block copolymers by combining the ROP and SCTP mechanisms. (b) SEC trace of the studied polymers obtained through smart synthesis in THF calibrated with polystyrene standards. (c) $^1$H NMR spectrum with peak designation and (d) DOSY NMR spectrum of $PF_{18}$-*b*-$PDL_{36}$ in $CDCl_3$ (The polymerization reactions were conducted in [TBD]:[4-iodobenzyl alcohol]$_0$:[*δ*-DL]$_0$:[HexFL]$_0$ = 1 : 1 : 60 : 18 at 25 °C in bulk for ROP and −10 °C in THF for SCTP).

reactions involving ring-opening alternating copolymerization (ROAC) of epoxide (EGE) and cyclic anhydrides (PA or AA) with SCTP of conjugated PF opens up the smart one pot synthetic strategy of PF-based conjugated BCPs (Fig. S4-7, Supporting Information). Our synthetic strategy works efficiently in constructing diverse PF-based BCPs as it acts straightforward, and functions facile in regulating the molecular blocks with desired physical properties. Through smart synthetic approach, we synthesized series of PF-based BCPs namely $PF_{18}$-*b*-$PDL_{13}$, $PF_{18}$-*b*-$PDL_{24}$, $PF_{18}$-*b*-$PDL_{36}$, $PF_{18}$-*b*-(PA-*alt*-EGE)$_{20}$, and $PF_{18}$-*b*-(AA-*alt*-EGE)$_{20}$, which represents the ease and flexibility in attaining desired degree of polymerization without any purification steps. We believe that our smart synthetic approach reducing the synthesis cost, time, solvent toxicity, and these credible features adding limelight to the path of commercialization and facile solution-processable wearable electronics.

Although we prepared series of BCPs, we focus primitively on $PF_{18}$-*b*-$PDL_n$ as our main theme of research is to fabricate bio-derived stretchable wearable LEDs. The chemical compositions of $PF_{18}$-*b*-$PDL_n$ were analyzed and confirmed by $^1$H, $^{13}$C, and 2D NMR spectra (Figs. S8–S13, Supporting Information). In the $^1$H NMR spectrum (Fig. 1c), the proton signals originating from the hexyl side chain on the PF block (peaks a, b, and c) and the main chain of the PDL block (peaks d, e, f, and g) were clearly observed for $PF_{18}$-*b*-$PDL_{36}$. The $^1$H, $^{13}$C, and 2D NMR peak positions and their peak integration values for all the BCPs are in a good agreement with the chemical structures and target molecular weights. Diffusion ordered spectroscopy (DOSY) NMR analysis, a powerful tool for accurately identifying individual NMR spectra from a mixture of various chemical species, was performed to determine the capability of the novel synthesis for producing a single type of BCP. The representative DOSY NMR spectrum of $PF_{18}$-*b*-$PDL_{36}$ (Fig. 1d) revealed only a single diffusion peak, which proves the smart one-pot synthesis only produced the copolymer virtually without side products. In contrast, two diffusion peaks were observed for a mixture of PF and PDL homopolymers (Fig. S14, Supporting Information). The NMR spectra and SEC traces suggested that well-defined BCPs are produced through the novel smart synthesis process. The novel synthesis is a simple, high yielding (typically 65%–67%),[2,3,24,30,31] and a short reaction (~2h); thus, this method is beneficial for the mass production of bio-derived BCPs.

### 3.2. Morphologies and optical properties of PF-b-PDL thin films

The thermal behavior of $PF_{18}$-*b*-$PDL_n$ were examined through thermogravimetric analysis (TGA) (Fig. S15, Supporting Information) and differential scanning calorimetry (DSC) (Fig. S16, Supporting Information) under a nitrogen atmosphere. The thermal parameters are summarized in Table S3 (Supporting Information). The homopolymer of PDL and PF revealed glass transition temperatures ($T_g$) at − 55.2 and 69.1 °C, respectively. As displayed in Fig. S16 (Supporting Information), each $PF_{18}$-*b*-$PDL_n$ copolymers exhibited two $T_g$, which originated from PDL and PF, respectively. The existence of individual phase transitions indicated the immiscibility of the PF and PDL blocks. Thus, PF and PDF segregated into separate domains.

The thin film morphology of $PF_{18}$-*b*-$PDL_n$ copolymers was investigated through synchrotron grazing-incidence wide-angle X-ray scattering (GIWAXS) measurements on as-cast and thermally annealed films (120 °C in vacuum for 1 day). As for PF homopolymer ($PF_{18}$), the as-cast film revealed a featureless data but the thermally annealed film revealed a set of weak crystalline peaks (Fig. S17a,b, Supporting Information). BCPs crystalline peaks attributed to the formation of an orthorhombic crystalline structure similar to that of poly(9,9-di-*n*-octyl-2,7-fluorene) (PFO).[28] In addition, a weak peak at approximately 16.8° in both out-of-plane and in-plane directions was observed with a *d*-spacing value of 4.2 Å, which evidenced the existence of $\pi$-$\pi$ stacking between PF chains. However, the relatively weak peak intensities suggest low PF crystallinity inside the annealed film. A similar result is observed for $PF_{18}$-*b*-$PDL_{13}$ (Fig. S17c,d, Supporting Information), with a minor difference in the annealed film that the scattering peaks are even weaker than PF homopolymer to suggest an even lower crystallinity. As for $PF_{18}$-*b*-$PDL_{24}$ and $PF_{18}$-*b*-$PDL_{36}$ (Fig. S17e-h, Supporting Information), the as-cast films revealed scattering peaks appearing as halos suggesting the orientation of PF crystals is not controlled. Post-annealing, peaks begins to take similar appearance to that of PF homopolymer, with $PF_{18}$-*b*-$PDL_{36}$ revealing a relatively more similar scattering pattern. Atomic force microscopy (AFM) was performed to further investigate the phase separation behavior. As shown in Fig. S18-S19, the as-cast films of PF

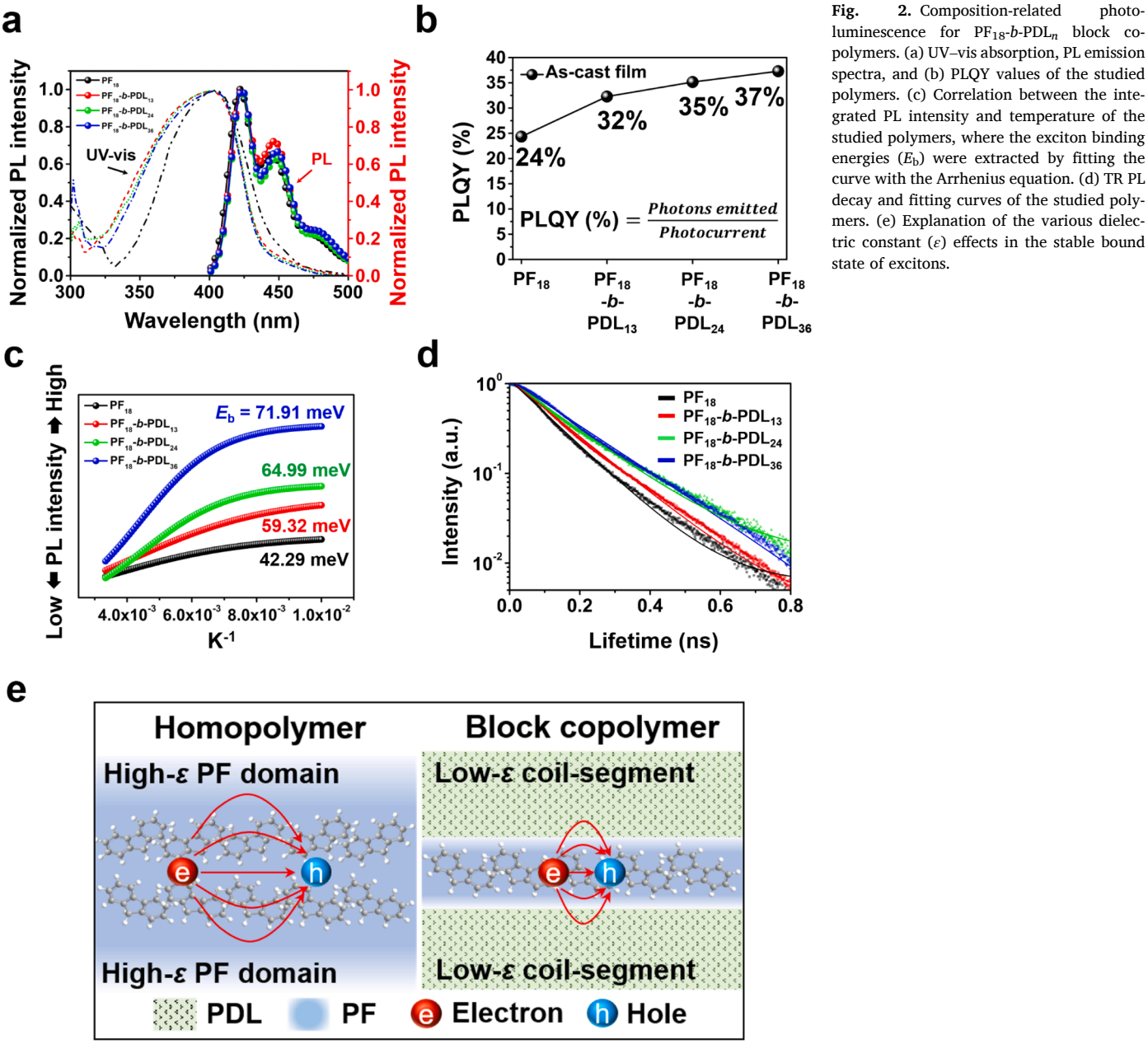


**Fig. 2.** Composition-related photoluminescence for $PF_{18}$-*b*-$PDL_n$ block copolymers. (a) UV–vis absorption, PL emission spectra, and (b) PLQY values of the studied polymers. (c) Correlation between the integrated PL intensity and temperature of the studied polymers, where the exciton binding energies ($E_b$) were extracted by fitting the curve with the Arrhenius equation. (d) TR PL decay and fitting curves of the studied polymers. (e) Explanation of the various dielectric constant ($\varepsilon$) effects in the stable bound state of excitons.

homopolymer and copolymers were featureless but a fibrillar structure was clearly observed on the surface of thermally annealed films for all BCPs. GIWAXS results ascertains the observed fibril morphological features originating from the tight packing of the PF blocks promoted by intermolecular $\pi$–$\pi$ interaction, and linked PDL blocks offers amorphous matrix around the PF fibers.

To investigate the correlation between the conformation and optical properties of the studied polymers, the ultraviolet–visible (UV–vis) absorption and photoluminescence (PL) spectra of the as-cast films were evaluated (Fig. 2a) and summarized in Table S4. The UV–vis absorption spectra of the as-cast films revealed both PF homopolymer and $PF_{18}$-*b*-$PDL_n$ copolymers to exhibit $\pi$–$\pi^*$ transition occurring at a wavelength of ~ 403 nm. The PL spectra of PF homopolymer and $PF_{18}$-*b*-$PDL_n$ copolymers did not reveal obvious differences between the as-cast and annealed states (Fig. S20), which confirmed that the PF chain conformation in the BCPs and PF homopolymer remains unaffected by thermal annealing. To confirm the luminescence properties, PLQY of the as-cast thin films were evaluated (Fig. 2b). The conjugated BCPs exhibited higher PLQY (32%–37%) than that of PF homopolymer (24%), which confirmed the superior luminescent property of the bio derived BCPs. These results complied well with previous studies.[22,24] A higher PLQY is correlated to a larger EBE,[38,39] which indicates more frequent radiative recombination of excitons occurring in BCP films at room temperature.

### 3.3. The correlation between PLQY and EBE

Excitons are one of the important factors that determine the overall performance of an LED device.[40–42] PLQY increments with conjugated molecularly designed BCP systems dedicates EBE modification and it is a critical factor in the LED device performance.[39,43] Therefore, temperature-dependent PL measurements were conducted on PF homopolymer and BCPs to quantify their EBE. Both homopolymer and BCPs exhibited a rapid decrease in their PL intensities with increasing temperature from 100 to 300 K (Fig. S21), which is governed by the strong screening effects eventually establishing a weak attractive force between electrons and holes in the exciton.[44,45] Furthermore, the integrated PL intensity was fitted with the Arrhenius equation [Equation (1); see Supporting Information] to obtain exciton binding energies (EBE) of 42.29, 59.32, 64.99, and 71.91 meV for $PF_{18}$, $PF_{18}$-*b*-$PDL_{13}$, $PF_{18}$-*b*-$PDL_{24}$, and $PF_{18}$-*b*-$PDL_{36}$, respectively (Fig. 2c). With decreasing molecular weight of PDL in the BCPs, EBE and PL is quenched causing detrimental effects on radiative recombination of photogenerated charges. The resulting PL and EBE trends are consistent with the PLQY results demonstrating the consistency of the as-synthesized bio-derived BCPs in terms of luminescence stability. Moreover, the time-resolved PL (TR PL) spectra (Fig. 2d) and the kinetics were analyzed to investigate the exciton recombination dynamics. All studied samples showing the typical exponentially decay behavior of PL intensities. On fitting the exponential decay curve, PF homopolymer exhibited a lifetime ($\tau_{avg}$) of 0.117 ns (Table S5). $PF_{18}$-*b*-$PDL_{13}$, $PF_{18}$-*b*-$PDL_{24}$, and $PF_{18}$-*b*-$PDL_{36}$ exhibited longer $\tau_{avg}$ of 0.137, 0.155, and 0.169 ns, respectively. Rapid dissociation and the separation of exciton recombination resulted in a rapid decline in the magnitudes of the fast component ($\tau_1$) (consider correcting the fast component!) (the fitting of exponential function is shown in the Supporting Information). It is well known that declining $\tau_{avg}$ values implies the electrons in the excited state transitioned to the ground state, which enhanced the non-radiative transition ratio.[46,47] $\tau_{avg}$ of $PF_{18}$-*b*-$PDL_n$ copolymers are longer than that of the PF homopolymer because their higher EBE stabilize the bound state. According to previous studies, extremely high EBE can be achieved in crystalline emissive materials by adding low-dielectric-constant ($\varepsilon$) organic components.[44] The presence of low-dielectric PDL blocks induces a weak screening effect and increases the attractive force between electrons and holes. In other words, bio derived PDL blocks significantly suppresses the non-radiative recombination and considerably enhance the magnitude of EBE. Therefore, these results indicate that EBE is considerably enhanced by incorporating PDL blocks, as illustrated in Fig. 2e. From the above discussion, we claim that PLQY promotion in the conjugated BCP is attributed to the stable bound state for the excitons induced by low dielectric PDL block. Our finding reveals the potential of one pot synthesized sustainable bio-derived BCPs in generating better eco-friendly photoluminescence material with intrinsic flex-stretch endurance. Bio-derived BCPs qualified the major preliminary requirements such as good photoluminescence and mechanical robustness allowing them for stretchable wearable LED device fabrication.

### 3.4. Fabrication and investigation of a stretchable touch-responsive LEDs

The stretchable and touch-responsive LED devices of PF homopolymer and BCPs were fabricated based on the architecture of polyurethane (PU)/poly(3,4-ethylenedioxythiophene)-poly(styrenesulfonate) (PEDOT: PSS) with poly(ethylene glycol) (PEO) (PEDOT:PSS/PEO)/ $PF_{18}$-*b*-$PDL_n$/poly(ethylene terephthalate) (PET)/PU with a silver nanowire electrode PU@AgNWs, as displayed in Fig. 3a and energy level diagram was exhibited in Fig. S22. The realization of these devices involved the following concepts. First, only elastic materials capable of withstanding strain were used. Second, a PET spacer was implanted between the upper electrode and the emissive layer. Therefore, the device only emits light when pressure is applied to the upper electrode. As displayed in Fig. 3b, the instantaneous light emission in the regions contacted by a wrench, and emission under 150% strain of $PF_{18}$-*b*-$PDL_{13}$ LED devices are observed. The as fabricated conformable device is patchable and easy to attach and peel without any device failure or degradation. Mechanically stable characteristics enabled stretchable and touch-responsive LEDs integration with finger joints which responds by lighting brilliantly on physical contact between the joint and device upon bending motion.

The luminescence–voltage (*L*–*V*), current density–voltage (*J*–*V*), and current efficiency–voltage (CE–*V*) characteristics are displayed in Fig. 3c,d and S16. The performance of the optimized devices is summarized in Table 1. As-cast devices with $PF_{18}$-*b*-$PDL_n$ as the emissive layer showed higher EQE (0.05%–0.10%) than using PF homopolymer ($EQE_{PF,as\text{-}cast}$ = 0.03%) and commercial PFO homopolymer ($EQE_{PFO,as\text{-}cast}$ = 0.034%), as presented in Table 1. Based on higher PLQY and EBE of $PF_{18}$-*b*-$PDL_n$, they possess more stable bound states and higher photon emission efficiencies than PF and PFO homopolymers. It is worth noting that both current density and EQE declines with increasing length of PDL block (Fig. S23, Supporting Information). The decline in current density is unfavorable to the recombination event, which results in greatly suppressed emission of $PF_{18}$-*b*-$PDL_{24}$ and $PF_{18}$-*b*-$PDL_{36}$ devices. Interestingly, $PF_{18}$-*b*-$PDL_{24}$ and $PF_{18}$-*b*-$PDL_{36}$ devices stop emitting photons once thermally annealed. $PF_{18}$-*b*-$PDL_{24}$ and $PF_{18}$-*b*-$PDL_{36}$ devices displays severely deteriorated emission and current density on thermal annealing due to the random orientations occurred with the crystalline block region which is evidenced with our AFM measurements. Hence, the overall resistance within the emission layer significantly increases and retards the device performance and operation. In contrast, $PF_{18}$-*b*-$PDL_{13}$, which has the shortest PDL block of all BCPs, possesses a relatively lower crystallinity. Among synthesized BCPs, the lower resistance offered by $PF_{18}$-*b*-$PDL_{13}$ emissive layer facilitates the current flow, and it additionally functions with intrinsically high EBE for optimal operation. Finally, the optimized device with thermal annealing treatment with the shortest PDL block ($PF_{18}$-*b*-$PDL_{13}$) exhibited a highly enhanced performance, with a maximum EQE of ~ 0.33% (at 18 V), which is 6 times higher than that of annealed PF (EQE = 0.05%) and annealed PFO (EQE = 0.05%) homopolymer LED devices.

To understand the correlation between mechanical stretch deformation and device performance based on PDL block lengths are characterized with optical microscopy (OM) of the annealed homopolymer and BCP emissive thin films (Fig. S24). Furthermore, Fig. S25 displays the photographs of the annealed homopolymer and BCP devices

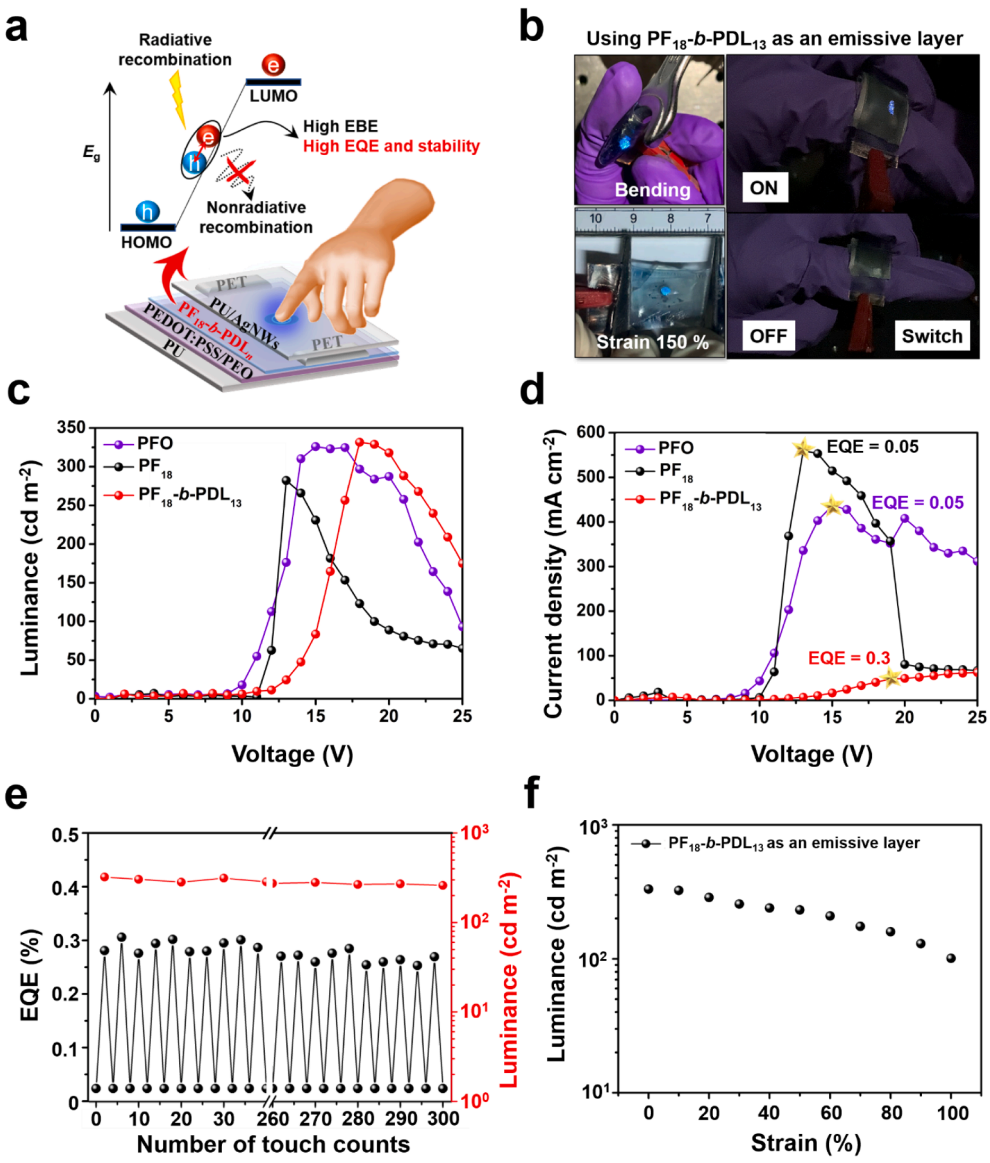


**Fig. 3.** Schematic diagrams and electroluminescence spectra of touch-responsive LEDs. (a) Schematic of the touch-responsive LEDs. (b) Photograph of the bend in contact with the wrench (irregular complex surface), which was stretched to 150% strain, and attached by the finger using $PF_{18}$-*b*-$PDL_{13}$ as an emissive layer (at 19 V). (c) *L*–*V* and (d) *J*–*V* characteristics of the touch-responsive LEDs. (e) Durability results for the luminance and EQE characteristics and (f) luminance of the touch-responsive LEDs under a uniaxial strain of 0%–100% when using $PF_{18}$-*b*-$PDL_{13}$ as an emissive layer (at 19 V).

**Table 1**
The molecular characteristics, photoelectric properties, and device performance of studied samples.

| Sample[a] | Molecular characteristics[b] | | | Photoelectric properties | | | Device performance(As-cast film)[c] | | | Device performance(Annealed film)[c] | | |
|---|---|---|---|---|---|---|---|---|---|---|---|---|
| | $M_{n,NMR}$(kDa) | $Đ$ | $\delta$-DL(wt %) | PLQY (%) | EBE (meV) | $\tau_{avg}$ | $L_{max}$(cd m$^{-2}$) | $CE_{max}$(cd A$^{-1}$) | EQE (%) | $L_{max}$(cd m$^{-2}$) | $CE_{max}$(cd A$^{-1}$) | EQE (%) |
| PFO | 10.0 | ~2.00 | 0 | – | – | – | 254 | 0.075 | 0.034 | 326 | 0.093 | 0.050 |
| $PF_{18}$ | 6.3 | 1.32 | 0 | 24.33 | 42.29 | 0.117 | 214 | 0.066 | 0.039 | 282 | 0.098 | 0.051 |
| $PF_{18}$-*b*-$PDL_{13}$ | 7.4 | 1.23 | 30 | 32.28 | 59.32 | 0.137 | 321 | 0.224 | 0.104 | 331 | 0.788 | 0.329 |
| $PF_{18}$-*b*-$PDL_{24}$ | 10.1 | 1.25 | 40 | 35.16 | 64.99 | 0.155 | 109 | 0.168 | 0.086 | – | – | – |
| $PF_{18}$-*b*-$PDL_{36}$ | 12.8 | 1.31 | 48 | 37.29 | 71.91 | 0.169 | 42 | 0.130 | 0.054 | – | – | – |

Abbreviations: $\delta$-DL, $\delta$-decanolactone; PLQY, photoluminance quantum yield; EBE, exciton binding energy; $\tau_{avg}$, lifetime value; $L_{max}$, the maximum of luminance; $CE_{max}$, the maximum of current efficiency; EQE, external quantum efficiency. [a]The samples were used as an emissive layer of the LED [b]The polymerization reactions were conducted in [TBD]:[4-iodobenzyl alcohol]$_0$:[$\delta$-DL]$_0$:[HexFL]$_0$ = 1 : 1 : 60 : 18 under 25 °C in bulk for ROP and − 10 °C in THF for SCRP. The molecular weights were determined from $^1$H NMR spectra through a comparison of the relative intensities of the polymer and initiator peaks ($\delta$(PF) = 2.21 ppm, $\delta$(PDL) = 4.87 ppm, $\delta$(initiator) = 5.18 ppm). [c]The device performances were recorded at the highest EQE voltage. *Device structure: PU / PEDOT:PSS / sample / PET / PU @ AgNWs. *Annealing condition: annealing at 120 °C in vacuum for 1 day. *PFO is a commercial polymer as a control group in the experiment.

emitting light at 19 V under 0% to 200% strain. Interestingly, only PF and $PF_{18}$-*b*-$PDL_{13}$ devices are functional whereas $PF_{18}$-*b*-$PDL_{24}$ and $PF_{18}$-*b*-$PDL_{36}$ devices, despite exhibiting improved deformability, suffer device failure due to overwhelming amount of PDL that induces high resistance. $PF_{18}$-*b*-$PDL_{13}$ devices works promising even under stretched states revealing the importance and reliability of the as synthesized bio-derived BCPs on comparison to homopolymer. Apart from stretchable performance, $PF_{18}$-*b*-$PDL_{13}$ device shows the rapid ultra-efficient touch-response performance along with greater mechanical endurance which is affirmed by repetitive touch-response cycles. Our device demonstrates stable touch-responsive operation at nearly the same level for ~ 300 switch on–off cycles without any sudden decrease in luminance and EQE portrays the device structural integrity (Fig. 3e). The uniaxial strain of 0%–100% representing the survivability of our device and it can be comfortably inlaid in an array of wearable electronics (Fig. 3f). The device exhibits 13% decrease in luminance at 30% strain, and this indicates the device's wide operational window under high strain. Mechanical stretch endurance (0%−20%) under repetitive 100 stretch cycles showed 39% luminance losses (Fig. S26), which already exhibit more stability than current reports.[48–51] In particular, the device retains comparable performance to 40% strain with only 34% decrease in luminance for 50 stretching cycles, thereby demonstrating its stability excellence (Fig. S26).Taking advantage of scalable one pot smart synthesized bio-derived BCPs, we successfully fabricated fully solution processable wearable LED device capable of working under higher strain % with outstanding flex-stretch endurance. Our future research direction involves preparing eco-friendly BCPs through one pot smart synthesis to employ them in a wide spectrum of eco-friendly wearable stretchable optoelectronics without sacrificing the device efficiency and stability.

## 4. Conclusions

In summary, we successfully prepared a series of PF-based bio-derived BCPs, namely $PF_{18}$-*b*-$PDL_n$, through a scalable smart one-pot synthesis. A commercially available difunctional initiator was used to induce both ROP and SCTP of PDL and PF blocks, respectively. The smart polymerization procedure was used for quick and efficient synthesis of BCPs with various PDL lengths controlled by varying the polymerization time. Moreover, we determined that the BCP strategy can considerably enhance EBE compared to PF due to the incorporating of a short insulating PDL segment. The $PF_{18}$-*b*-$PDL_n$ devices exhibited excellent radiative recombination because of their stable bound state induced by high EBE. Among synthesized BCPs, $PF_{18}$-*b*-$PDL_{13}$ achieves the highest EQE = 0.33%, which is 6 times higher than that of the PF and PFO homopolymers. Therefore, mechanically robust highly flexible and stretchable touch-responsive LEDs with ultra-high efficiency were fabricated with $PF_{18}$-*b*-$PDL_{13}$ capable of integrating with human finger, curved joints and smart garments. The findings of this study possibly elevated the conjugated BCPs importance with robust stretchable wearable LED fabrication and our one pot smart synthesis is anticipated to achieve impressive breakthroughs in forming diverse eco-friendly materials and wearable electronic fabrication.

## Declaration of Competing Interest

The authors declare that they have no known competing financial interests or personal relationships that could have appeared to influence the work reported in this paper.

## Acknowledgments

D. H. J. and B. J. R. contributed equally to this work. This work is supported by the Ministry of Science and Technology, Taiwan (MOST 106-2221-E-027-119-MY3, MOST 105-2221-E-027-134-, and MOST 104-2113-M-027-007-MY3), the JSPS Grant-in-Aid for Scientific Research (B) (19H02769), MEXT Grant-in-Aid for Scientific Research on Innovative Areas (Hybrid Catalysis for Enabling Molecular Synthesis on Demand; 18H04639 and 20H04798), JST CREST (JPMJCR19T4), Frontier Chemistry Center (Hokkaido University), Photo-excitonic Project (Hokkaido University), and Creative Research Institute (CRIS, Hokkaido University).

## Appendix A. Supplementary data

Supplementary data to this article can be found online at https://doi.org/10.1016/j.cej.2021.129421.

## References

[1] J.-T. Wang, K. Saito, H.-C. Wu, H.-S. Sun, C.-C. Hung, Y. Chen, T. Isono, T. Kakuchi, T. Satoh, W.-C. Chen, High-performance stretchable resistive memories using donor–acceptor block copolymers with fluorene rods and pendent isoindigo coils, NPG Asia Mater. 8 (8) (2016) e298.
[2] C.S. Fischer, M.C. Baier, S. Mecking, Enhanced brightness emission-tuned nanoparticles from heterodifunctional polyfluorene building blocks, J. Am. Chem. Soc. 135 (3) (2013) 1148–1154.
[3] J.-J. Li, J.-J. Wang, Y.-N. Zhou, Z.-H. Luo, Synthesis and characterization of polyfluorene-based photoelectric materials: the effect of coil segment on the spectral stability, RSC Adv. 4 (38) (2014) 19869–19877.
[4] Y.-Y. Yu, C.-Y. Huang, Morphological Transformation and Photophysical Properties of Polyfluorene-Based Luminescent Rod-Coil Block Copolymers, J. Nanomater. 2016 (2016).
[5] Y. Liu, L. Hua, S. Yan, Z. Ren, Halogenated π-conjugated polymeric emitters with thermally activated delayed fluorescence for highly efficient polymer light emitting diodes, Nano Energy 73 (2020), 104800.
[6] L. Hua, S.-K. Yan, Z.-J. Ren, Molecular design and device performance of thermally activated delayed fluorescent polymer materials, Acta. Polym. Sin. 51 (5) (2020) 457–468.
[7] C. Li, Y. Xu, Y. Liu, Z. Ren, Y. Ma, S. Yan, Highly efficient white-emitting thermally activated delayed fluorescence polymers: Synthesis, non-doped white OLEDs and electroluminescent mechanism, Nano Energy 65 (2019), 104057.
[8] C. Li, Z. Ren, X. Sun, H. Li, S. Yan, Deep-blue thermally activated delayed fluorescence polymers for nondoped solution-processed organic light-emitting diodes, Macromolecules 52 (6) (2019) 2296–2303.
[9] X. Zhao, K. Deng, F. Liu, X. Zhang, H. Yang, J. Peng, Z. Liu, L. Ma, B. Wang, H. Wei, Fabrication of conjugated amphiphilic triblock copolymer for drug delivery and fluorescence cell imaging, ACS Biomater. Sci. Eng. 4 (2) (2018) 566–575.
[10] K. Deng, X. Zhao, F. Liu, J. Peng, C. Meng, Y. Huang, L. Ma, C. Chang, H. Wei, Synthesis of Thermosensitive Conjugated Triblock Copolymers by Sequential Click Couplings for Drug Delivery and Cell Imaging, ACS Biomater. Sci. Eng. 5 (7) (2019) 3419–3428.
[11] Y.-C. Chiu, Y. Chen, C.-C. Kuo, S.-H. Tung, T. Kakuchi, W.-C. Chen, Synthesis, morphology, and sensory applications of multifunctional rod–coil–coil triblock copolymers and their electrospun nanofibers, ACS Appl. Mater. Interfaces 4 (7) (2012) 3387–3395.
[12] Z. Jin, H. Fan, Self-assembly of nanostructured block copolymer nanoparticles, Soft Matter 10 (46) (2014) 9212–9219.
[13] Y.-H. Lee, W.-C. Yen, W.-F. Su, C.-A. Dai, Self-assembly and phase transformations of π-conjugated block copolymers that bend and twist: from rigid-rod nanowires to highly curvaceous gyroids, Soft Matter 7 (21) (2011) 10429–10442.
[14] K. Saito, T. Isono, H.-S. Sun, T. Kakuchi, W.-C. Chen, T. Satoh, Rod–coil type miktoarm star copolymers consisting of polyfluorene and polylactide: precise synthesis and structure–morphology relationship, Polym. Chem. 6 (39) (2015) 6959–6972.
[15] D. Kipp, J. Mok, J. Strzalka, S.B. Darling, V. Ganesan, R. Verduzco, Rational Design of Thermally Stable Bicontinuous Donor/Acceptor Morphologies with Conjugated Block Copolymer Additives, *ACS Macro Lett.* 4 (9) (2015) 867–871.
[16] Y. Tao, B. Ma, R.A. Segalman, Self-assembly of rod− coil block copolymers and their application in electroluminescent devices, Macromolecules 41 (19) (2008) 7152–7159.
[17] X. Jiang, S. Liu, H. Ma, A.-K.-Y. Jen, High-performance blue light-emitting diode based on a binaphthyl-containing polyfluorene, Appl. Phys. Lett. 76 (14) (2000) 1813–1815.
[18] X. Gong, P.K. Iyer, D. Moses, G.C. Bazan, A.J. Heeger, S.S. Xiao, Stabilized blue emission from polyfluorene-based light-emitting diodes: elimination of fluorenone defects, Adv. Funct. Mater. 13 (4) (2003) 325–330.
[19] I.O. Huyal, U. Koldemir, T. Ozel, H.V. Demir, D. Tuncel, On the origin of high quality white light emission from a hybrid organic/inorganic light emitting diode using azide functionalized polyfluorene, J. Mater. Chem. 18 (30) (2008) 3568–3574.
[20] L. Hu, Z. Wu, X. Wang, Y. Ma, T. Guo, L. Ying, J. Peng, Y. Cao, Deep-blue light-emitting polyfluorenes with asymmetrical naphthylthio-fluorene as Chromophores, *J. Polym. Sci., Part A-1*, Polym. Chem. 57 (2) (2019) 171–182.
[21] Q. Feng, S. Xie, K. Tan, X. Zheng, Z. Yu, L. Li, B. Liu, B. Li, M. Yu, Y. Yu, Conjugated Nanopolymer Based on a Nanogrid: Approach toward Stable Polyfluorene-Type Fluorescent Emitter for Blue Polymer Light-Emitting Diodes, ACS Appl. Mater. Interfaces 1 (9) (2019) 2441–2449.

[22] H.-C. Hsieh, C.-C. Hung, K. Watanabe, J.-Y. Chen, Y.-C. Chiu, T. Isono, Y.-C. Chiang, R.R. Reghu, T. Satoh, W.-C. Chen, Unraveling the stress effects on the optical properties of stretchable rod-coil polyfluorene-poly (n-butyl acrylate) block copolymer thin films, Polym. Chem. 9 (27) (2018) 3820–3831.
[23] R.M. Van Horn, M.R. Steffen, D. O'Connor, Recent progress in block copolymer crystallization, Polym. Crystallization 1 (4) (2018), e10039.
[24] A.-N. Au-Duong, C.-C. Wu, Y.-T. Li, Y.-S. Huang, H.-Y. Cai, I. Jo Hai, Y.-H. Cheng, C.-C. Hu, J.-Y. Lai, C.-C. Kuo, Synthetic Concept of Intrinsically Elastic Luminescent Polyfluorene-Based Copolymers via RAFT Polymerization, Macromolecules 53 (2020) 4030–4037.
[25] D.-H. Jiang, S. Kobayashi, C.-C. Jao, Y. Mato, T. Isono, Y.-H. Fang, C.-C. Lin, T. Satoh, S.-H. Tung, C.-C. Kuo, Light Down-Converter Based on Luminescent Nanofibers from the Blending of Conjugated Rod-Coil Block Copolymers and Perovskite through Electrospinning, Polym. 12 (1) (2020) 84.
[26] P.E. Shaw, A. Ruseckas, I.D. Samuel, Exciton diffusion measurements in poly (3-hexylthiophene), Adv. Mater. 20 (18) (2008) 3516–3520.
[27] M. Sim, J. Shin, C. Shim, M. Kim, S.B. Jo, J.-H. Kim, K. Cho, Dependence of Exciton diffusion length on crystalline order in conjugated polymers, J. Phys. Chem. C 118 (2) (2014) 760–766.
[28] H.C. Hsieh, J.Y. Chen, W.Y. Lee, D. Bera, W.C. Chen, Stretchable fluorescent polyfluorene/acrylonitrile butadiene rubber blend electrospun fibers through physical interaction and geometrical confinement, Macromol. Rapid Commun. 39 (5) (2018) 1700616.
[29] H.-C. Hsieh, N. Wu, T.-H. Chuang, W.-Y. Lee, J.-Y. Chen, W.-C. Chen, Eco-friendly Polyfluorene/Poly (butylene succinate) Blends and Their Electronic Device Application on Biodegradable Substrate, ACS Appl. Polym. Mater. 2 (2020) 2469–2476.
[30] Y. Tian, C.-Y. Chen, H.-L. Yip, W.-C. Wu, W.-C. Chen, A.-K.-Y. Jen, Synthesis, nanostructure, functionality, and application of polyfluorene-block-poly (N-isopropylacrylamide) s, Macromolecules 43 (1) (2010) 282–291.
[31] S. Huber, S. Mecking, Straightforward Synthesis of Conjugated Block Copolymers by Controlled Suzuki-Miyaura Cross-Coupling Polymerization Combined with ATRP, Macromolecules 52 (15) (2019) 5917–5924.
[32] S. Kobayashi, K. Fujiwara, D.-H. Jiang, T. Yamamoto, K. Tajima, Y. Yamamoto, T. Isono, T. Satoh, Suzuki-Miyaura catalyst-transfer polycondensation of triolborate-type fluorene monomer: toward rapid access to polyfluorene-containing block and graft copolymers from various macroinitiators, Polym. Chem. 11 (42) (2020) 6832–6839.
[33] Y.Y. Kim, B.J. Ree, M. Kido, Y.G. Ko, R. Ishige, T. Hirai, D. Wi, J. Kim, W.J. Kim, A. Takahara, High-Performance n-Type Electrical Memory and Morphology-Induced Memory-Mode Tuning of a Well-Defined Brush Polymer Bearing Perylene Diimide Moieties, Adv. Electron. Mater. 1 (10) (2015) 1500197.
[34] B. Lee, Y.-H. Park, Y.-T. Hwang, W. Oh, J. Yoon, M. Ree, Ultralow-k nanoporous organosilicate dielectric films imprinted with dendritic spheres, Nat. Mater. 4 (2) (2005) 147–150.
[35] B.J. Ree, Y. Satoh, T. Isono, T. Satoh, Bicyclic Topology Transforms Self-Assembled Nanostructures in Block Copolymer Thin Films, Nano Lett. 20 (9) (2020) 6520–6525.
[36] M.J.M.r.c. Ree, Probing the Self-Assembled Nanostructures of Functional Polymers with Synchrotron Grazing Incidence X-Ray Scattering, Macromol. Rapid Commun. 35 (10) (2014) 930–959.
[37] S. Kobayashi, K. Fujiwara, D.-H. Jiang, T. Yamamoto, K. Tajima, Y. Yamamoto, T. Isono, T. Satoh, Suzuki-Miyaura Catalyst-Transfer Polycondensation of Triolborate-Type Fluorene Monomer: Toward Rapid Access to Polyfluorene-Containing Block and Graft Copolymers from Various Macroinitiators, Polym. Chem. 00 (2020) 1–3.
[38] H. Wang, X. Zhang, Q. Wu, F. Cao, D. Yang, Y. Shang, Z. Ning, W. Zhang, W. Zheng, Y. Yan, Trifluoroacetate induced small-grained CsPbBr 3 perovskite films result in efficient and stable light-emitting devices, Nat. Commun. 10 (1) (2019) 1–10.
[39] H.C. Woo, J.W. Choi, J. Shin, S.-H. Chin, M.H. Ann, C.-L. Lee, Temperature-dependent photoluminescence of CH3NH3PbBr 3 perovskite quantum dots and bulk counterparts, J. Phys. Chem. Lett. 9 (14) (2018) 4066–4074.
[40] R.A. Janssen, J. Nelson, Factors limiting device efficiency in organic photovoltaics, Adv. Mater. 25 (13) (2013) 1847–1858.
[41] S.D. Stranks, R.L. Hoye, D. Di, R.H. Friend, F. Deschler, The physics of light emission in halide perovskite devices, Adv. Mater. 31 (47) (2019) 1803336.
[42] B. Yang, K. Han, Charge-carrier dynamics of lead-free halide perovskite nanocrystals, Acc. Chem. Res. 52 (11) (2019) 3188–3198.
[43] J. Maultzsch, R. Pomraenke, S. Reich, E. Chang, D. Prezzi, A. Ruini, E. Molinari, M. Strano, C. Thomsen, C. Lienau, Exciton binding energies in carbon nanotubes from two-photon photoluminescence, Phys. Rev. B 72 (24) (2005), 241402.
[44] B. Cheng, T.-Y. Li, P. Maity, P.-C. Wei, D. Nordlund, K.-T. Ho, D.-H. Lien, C.-H. Lin, R.-Z. Liang, X. Miao, Extremely reduced dielectric confinement in two-dimensional hybrid perovskites with large polar organics, Commun. Phys. 1 (1) (2018) 1–8.
[45] Z.A. Lan, G. Zhang, X. Chen, Y. Zhang, K.A. Zhang, X. Wang, Reducing the Exciton Binding Energy of Donor–Acceptor-Based Conjugated Polymers to Promote Charge-Induced Reactions, *Angew.e*, Chem. Int. 58 (30) (2019) 10236–10240.
[46] L. Wang, C. McCleese, A. Kovalsky, Y. Zhao, C. Burda, Femtosecond time-resolved transient absorption spectroscopy of CH3NH3PbI3 perovskite films: evidence for passivation effect of PbI2, J. Am. Chem. Soc. 136 (35) (2014) 12205–12208.
[47] M. Leng, Y. Yang, Z. Chen, W. Gao, J. Zhang, G. Niu, D. Li, H. Song, J. Zhang, S. Jin, Surface passivation of bismuth-based perovskite variant quantum dots to achieve efficient blue emission, Nano Lett. 18 (9) (2018) 6076–6083.
[48] D.-H. Jiang, Y.-C. Liao, C.-J. Cho, L. Veeramuthu, F.-C. Liang, T.-C. Wang, C.-C. Chueh, T. Satoh, S.-H. Tung, C.-C. Kuo, Facile Fabrication of Stretchable Touch-Responsive Perovskite Light-Emitting Diodes Using Robust Stretchable Composite Electrodes, ACS Appl. Mater. Interfaces 12 (12) (2020) 14408–14415.
[49] C.C. Jao, J.R. Chang, C.Y. Ya, W.C. Chen, C.J. Cho, J.H. Lin, Y.C. Chiu, Y. Zhou, C. C. Kuo, Novel stretchable light-emitting diodes based on conjugated-rod block elastic-coil copolymers, Polym, Int, 2020.
[50] S.G.R. Bade, X. Shan, P.T. Hoang, J. Li, T. Geske, L. Cai, Q. Pei, C. Wang, Z. Yu, Stretchable Light-Emitting Diodes with Organometal-Halide-Perovskite–Polymer Composite Emitters, Adv. Mater. 29 (23) (2017) 1607053.
[51] J. Liang, L. Li, X. Niu, Z. Yu, Q. Pei, Elastomeric polymer light-emitting devices and displays, Nat. Photonics 7 (10) (2013) 817–824.